Three-dimensional spatiotemporal pulse characterization with an acousto-optic pulse shaper and a Hartmann–Shack wavefront sensor

Seth L. Cousin,[1] Juan M. Bueno,[2] Nicolas Forget,[3] Dane R. Austin,[1,*] and J. Biegert[1,4]

[1]*ICFO—Institut de Ciencies Fotoniques, Mediterranean Technology Park, 08860 Castelldefels, Barcelona, Spain*

[2]*Laboratorio de Óptica, Universidad de Murcia, Campus de Espinardo (Ed. 34), 30100 Murcia, Spain*

[3]*FASTLITE, Centre Scientifique d'Orsay—Bât. 503—BP 45, 91401 Orsay, France*

[4]*ICREA—Institució Catalana de Recerca i Estudis Avançats, 08010 Barcelona, Spain*

**Corresponding author: dane.austin@icfo.es*

Received June 1, 2012; revised June 1, 2012; accepted June 28, 2012;
posted July 2, 2012 (Doc. ID 165763); published July 31, 2012

We demonstrate a simplified arrangement for spatiotemporal ultrashort pulse characterization called Hartmann–Shack assisted, multidimensional, shaper-based technique for electric-field reconstruction. It employs an acousto-optic pulse shaper in combination with a second-order nonlinear crystal and a Hartmann–Shack wavefront sensor. The shaper is used as a tunable bandpass filter, and the wavefronts and intensities of quasimonochromatic spectral slices of the pulse are obtained using the Hartmann–Shack wavefront sensor. The wavefronts and intensities of the spectral slices are related to one another using shaper-assisted frequency-resolved optical gating measurements, performed at particular points in the beam. This enables a three-dimensional reconstruction of the amplitude and phase of the pulse. We present some example pulse measurements and discuss the operating parameters of the device.

OCIS codes: 320.7100, 320.5540, 140.3295, 320.7080.

The characterization of femtosecond optical pulses is a central component of ultrafast technology and is routinely accomplished using techniques based in spectrography [1] or interferometry [2]. In their most basic forms, these methods ignore or average over any spatial variation in the temporal profile. However, spatiotemporal coupling occurs commonly in ultrafast optics, for example through misaligned dispersive elements or nonlinear pulse propagation [3]. The opportunities as well as the problems that arise from such coupling have motivated the extension of temporal characterization methods to the spatiotemporal domain. One common approach is to combine a temporal characterization of a point in the beam with a set of spectrally resolved wavefront measurements, obtained using lateral shearing interferometry [4], test-plus-reference interferometry [5], or a Hartmann–Shack wavefront sensor [6]. Since these extensions add complexity and alignment, it is worthwhile searching for more simple and robust implementations, particularly ones in which the optical elements play dual roles in both the temporal and spatial characterization.

In this Letter, we present such an implementation: Hartmann–Shack assisted, multidimensional, shaper-based technique for electric-field reconstruction (HAMSTER), which is based around an acousto-optic programmable dispersive filter (AOPDF) [7]. In combination with a second-order nonlinear crystal and a spectrometer, the AOPDF enables temporal characterization using a variety of methods; here we use baseband interferometric frequency-resolved optical gating (bFROG) [8]. The AOPDF can also be operated as a tunable bandpass filter, whose output is directed onto a Hartmann–Shack wavefront sensor [9,10]. In this way, a series of spatial intensity and phase profiles of quasimonochromatic spectral slices of the pulse is obtained. We demonstrate the device by characterizing angularly dispersed pulses from a Ti:sapphire amplifier.

Figure 1 shows a schematic of the device. The measurement plane M is relayed to the AOPDF by the telescope formed by $f = 500$ mm lenses L1 and L2. It is then relayed by the telescope formed by $f = 200$ mm lenses L3 and L4, via a flip-mounted mirror FM, to either the lenslet plane of the Hartmann–Shack wavefront sensor (Thorlabs WFS-150) or to iris I2. The point in the beam selected by I2 is used for temporal characterization and can be chosen by lateral translation of retroreflector R. A third 4-f telescope, consisting of $f = 500$ mm lens L5 and $f = 50$ mm lens L6, forms a 10× reduced image of the iris on the measurement plane on a 50 μm beta-barium borate crystal cut for type-I conversion. The $f = 50$ mm lens L7 images the generated sum-frequency beam onto the entrance slit of the spectrometer (Avantes AvaSpec-2048-USB2). Filter F (Schott BG39) removes the fundamental. The dispersion of lenses L1–L6 and the AOPDF are calibrated using a separate device or interferometry and compensated by the AOPDF during measurements. Note that the telescope L1–L2 is only necessary in order to

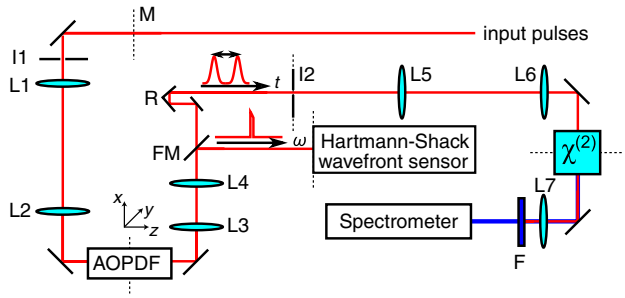

Fig. 1. (Color online) Schematic setup of the HAMSTER spatiotemporal measurement device; the acronyms are described in the text. Planes conjugate to the measurement plane M are indicated by dashed lines.

0146-9592/12/153291-03$15.00/0

measure the pulse at external plane M rather than at the AOPDF.

A measurement is performed by programming the AOPDF to act as a tunable bandpass filter, directing its output to the wavefront sensor, and sequentially acquiring the wavefronts of sufficiently narrow spectral slices across the bandwidth of the pulse. The spatial phase and intensity profiles (the latter inferred from the intensity of the focal spots formed by the lenslet array) are combined to form the three-dimensional spatiospectral electric field $E(x,y,\omega)A(\omega)\exp iB(\omega)$, up to unknown frequency-dependent scaling $A(\omega)$ and phase $B(\omega)$ factors. (While $A(\omega)$ could be inferred from the spectral response of the wavefront sensor and the AOPDF, it is more convenient to use the spectrum retrieved by the bFROG.) The AOPDF output is then directed to the temporal characterization arrangement. The point (x_0, y_0) selected by I2 for temporal characterization is located in the Hartmann–Shack images by sending an irised beam into the system such that it passes through I2. After inserting FM, this beam marks the selected point on the sensor. This calibration is independent of the incident beam direction and need only be performed once. The AOPDF is programmed to produce time-delayed and phase-shifted replicas for the bFROG measurement. Inversion of the bFROG trace [up to the second harmonic generation frequency-resolved optical gating (FROG) ambiguities of absolute phase and arrival time] yields $E(x_0, y_0, \omega)$, from which one obtains $A(\omega)$ and $B(\omega)$ and hence the full three-dimensional complex amplitude of the pulse. The direction of time ambiguity is resolved by applying a known phase using the AOPDF and repeating the measurement. Further Fourier transforms yield the profile in any combination of the spectral/temporal and spatial/transverse-wavenumber domains.

The pulse parameter restrictions introduced by the AOPDF and the wavefront sensor are quite acceptable in our implementation. At 800 nm, the AOPDF is capable of characterizing pulses with transform limits above 20 fs and durations below 500 fs [11], while the smallest obtainable spectral slice is 0.3 nm. The spatial aperture is 2 mm. The spatial resolution is limited by the pitch of the lenslet array of the wavefront sensor, in our case 146 μm. Two artifacts of the AOPDF can, in principle, worsen this. First, the device applies a group-delay-dependent displacement of the beam in the diffraction plane [12,13], which we take as the yz plane here. In our setup, this coupling is $v = 0.1$ μm/fs. This causes lateral movement of the replicas during the bFROG scan. The induced loss of spatial resolution is equal to the product of v and the bFROG delay range and is insignificant for the parameters considered here. Second, the wavelength tuning of the AOPDF depends on the input beam angle in the diffraction plane, necessitating a compromise between spectral resolution and angular acceptance in the diffraction plane. We measured this coupling to be 0.26 nm/mrad. Finally, inhomogeneity in the acoustic wave in the AOPDF can produce a spatial intensity modulation (approximately 10%) along the diffraction direction. This may be easily diagnosed by small translations of the AOPDF but cannot be easily eliminated.

As an example, we characterized pulses which had passed, with incident angle $58.1° \pm 0.2°$, through an N-SF11 equilateral prism located at the measurement plane. In accordance with the coupling between AOPDF incidence angle and wavelength described above, the dispersion was in the xz plane. The pulses were from a Ti:sapphire chirped-pulse amplification system, with 35 fs FWHM, center wavelength 795 nm, and $1/e^2$ beam radius 1.25 mm. Using a pulse shaper inside the amplifier, we applied a spectral phase of -1000 fs^2 to compensate for the dispersion of the center of the beam in the prism. The pulse energy incident upon the AOPDF was 9 μJ. The wavefronts were sampled at 2 nm increments, and a 0.4 mm diameter portion of the center of the beam was characterized by the bFROG. The reconstructed spatiotemporal profile, represented as a surface of half-maximum intensity, is shown in Fig. 2(a). The measured pulse front tilt is $6.63° \pm 0.05°$, consistent with the theoretical value [14] of $6.64° \pm 0.06°$ inferred using the incident angle. Another comparison with theory is the transverse chirp variation in the direction of angular dispersion, caused by propagation through different lengths of prism glass. The extracted quadratic spectral phase is plotted against x in Fig. 2(b), along with a linear fit (to the central part of the beam) of slope 510 ± 20 fs^2/mm. This compares well with the theoretical value of 507 ± 6 fs^2/mm. Otherwise, the pulse is nearly identical to that measured without the prism.

To observe the dispersive effect of propagation on the angularly dispersed beam, we moved the prism 70 mm forward of the object plane. The measured pulse is similar, but with an additional quadratic spectral phase of 1350 ± 80 fs^2/mm, implying a dispersion per unit length of 19.3 ± 1 fs^2/mm. This is consistent with the value of 19.1 ± 0.4 fs^2/mm expected from theory [15].

A general restriction of combining spectrally resolved wavefronts with a single temporal characterization is that the latter must contain all frequencies in the entire beam [5]. Our device offers a convenient way of alleviating this. By translating the retroreflector R in the transverse plane, we can select different points in the beam (x_n, y_n) to be temporally characterized. An unambiguous reconstruction is possible if the entire (x, y, λ) volume of the pulse is connected a combination of "moves," which may either use the spectrally resolved wavefronts and are constrained to a plane of fixed λ or use the temporal

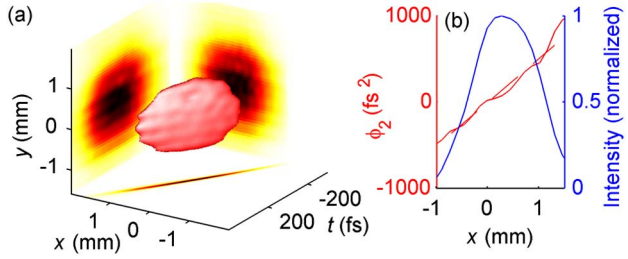

Fig. 2. (Color online) (a) Spatiotemporal intensity of the prism-dispersed pulse, represented as a surface of 50% peak intensity, with projections along the coordinate axes. (b) Measured quadratic spectral phase versus position along the axis of angular dispersion x (red, left axis) with linear fit (red dashed). Normalized intensity projected onto the x axis (blue, right axis).

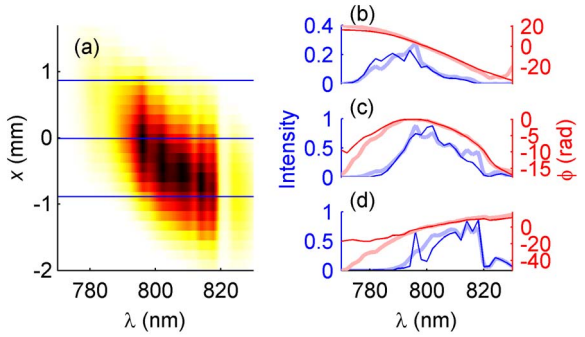

Fig. 3. (Color online) (a) Spatiospectral intensity profile of pulse measured 371 mm after the prism. The horizontal blue lines indicate the points temporally characterized by the bFROG. (b)–(d) Spectral intensity (blue, left axis) and phase (red, right axis) at the three temporally characterized points. Faint, thick lines show the final reconstructed profiles, while thin, dark lines show what is directly retrieved by the bFROG reconstruction.

characterizations and are constrained along one of the measurement points (x_n, y_n). To demonstrate this, we placed the prism 371 mm before the object plane of the HAMSTER. At this propagation distance, angular dispersion leads to a spatial chirp, and not all frequencies have sufficient intensity at the central point of the beam. Figure 3(a) shows the slice $y = 0$ through the spatiospectral intensity volume. We obtained bFROG measurements at the points indicated by the horizontal blue lines (all were at $y = 0$). As will generally be the case, there was some redundancy in the data since the spectra at these points have some overlap. The system is therefore overdetermined, and we use separate least-squares minimizations for the intensity and phase. The ambiguities present in each measurement—the aforementioned $A(\omega)$ and $B(\omega)$ for the wavefronts and their intensities, and the absolute phases, arrival times, and arbitrary scale factor for the bFROG reconstructions—are treated as free parameters. The phase equations are weighted by the local intensity. Both the intensity and phase equations may be robustly solved using a least-squares minimization. In Figs. 3(b)–3(d), the spectral intensity and phase reconstructed at each temporal characterization point is compared with that obtained directly from the bFROG measurements. The intensities agree except for a few isolated points caused by the reconstruction being close to the maximum temporal window of the bFROG, required for the dispersed, narrowband pulses. The phases agree except in places where the spectral intensity is low.

In summary, we have demonstrated three-dimensional spatiotemporal characterization of ultrashort pulses by combining a shaper-assisted FROG with a Hartmann–Shack wavefront sensor. Our setup exploits the growing availability of compact monolithic implementations of these devices to perform a task that normally requires a more complex and alignment-intensive setup.

The authors acknowledge support from the Spanish Ministerio De Ciencia E Innovacion (MICINN) through its Consolider Program (SAUUL—CSD 2007-00013) and "Participation in ELI" (CAC-2007-37) as well as through "Plan Nacional" (FIS2008-06368-C02-01) and the Catalan Agència de Gestió d'Ajuts Universitaris i de Recerca (AGAUR) with SGR 2009-2013. Funding from LASERLAB-EUROPE (228334) is gratefully acknowledged. D. R. A was supported by a Marie Curie Intra-European Fellowship (project 276556-BAXHHG).

References

1. D. Kane and R. Trebino, IEEE J. Quantum Electron. **29**, 571 (1993).
2. C. Iaconis and I. A. Walmsley, Opt. Lett. **23**, 792 (1998).
3. A. Zaïr, A. Guandalini, F. Schapper, M. Holler, J. Biegert, L. Gallmann, A. Couairon, M. Franco, A. Mysyrowicz, and U. Keller, Opt. Express **15**, 5394 (2007).
4. C. Dorrer, E. Kosik, and I. Walmsley, Appl. Phys. B **74**, s209 (2002).
5. P. Gabolde and R. Trebino, Opt. Express **12**, 4423 (2004).
6. E. Rubino, D. Faccio, L. Tartara, P. K. Bates, O. Chalus, M. Clerici, F. Bonaretti, J. Biegert, and P. Di Trapani, Opt. Lett. **34**, 3854 (2009).
7. P. Tournois, Opt. Commun. **140**, 245 (1997).
8. N. Forget, V. Crozatier, and T. Oksenhendler, J. Opt. Soc. Am. B **27**, 742 (2010).
9. B. Platt and R. V. Shack, Opt. Sci. Cent. Newsl. **5**, 15 (1971).
10. J. M. Bueno, B. Vohnsen, L. Roso, and P. Artal, Appl. Opt. **48**, 770 (2009).
11. S. L. Cousin, N. Forget, A. Grün, P. K. Bates, D. R. Austin, and J. Biegert, Opt. Lett. **36**, 2803 (2011).
12. D. J. McCabe, D. R. Austin, A. Tajalli, S. Weber, I. A. Walmsley, and B. Chatel, J. Opt. Soc. Am. B **28**, 58 (2011).
13. N. Krebs, R. A. Probst, and E. Riedle, Opt. Express **18**, 6164 (2010).
14. J. Hebling, Opt. Quantum Electron. **28**, 1759 (1996).
15. O. E. Martinez, J. P. Gordon, and R. L. Fork, J. Opt. Soc. Am. A **1**, 1003 (1984).